Biogeochemical Impacts of Storm and High Wind Events in the Southern Ocean

Olivia Kimbro, North Carolina State University

Mentors: Magdalena Carranza, Guillaume Liniger Summer 2026

Keywords: BGC Argo, Biogeochemical, Phytoplankton, SOCCOM, Carbon dioxide

ABSTRACT

The Southern Ocean (SO) is known for its major role in the world's carbon dioxide (CO_2) flux, being the second smallest ocean in the world, yet having the largest CO_2 intake of all other oceans. A critical source of CO_2 uptake in the SO is phytoplankton blooms. In the open ocean, away from major sources of nutrients, biological activity depends on upwelling, a process that can rapidly change the subsurface's properties. In this project, we use high frequency profiling BGC Argo floats to analyze high wind and storm-induced sub-surface biogeochemical properties in the SO. We aim to identify a high wind or storm event in the proximity of a high frequency profiling BGC Argo float to do this. We note a single event of interest across high frequency profiling floats in the SO, and suggest a high wind-induced phytoplankton bloom following the process of MLD deepening and shoaling. We also suggest detrainment during the stratification process. Our findings support the existing knowledge on storm-induced phytoplankton blooms, and emphasizes the need for increased high frequency profiling periods among floats.

1 INTRODUCTION

The Southern Ocean is recognized as the largest carbon sink, which is responsible for 40% of the global oceanic carbon uptake (Gruber et al. 2019). However, we lack a

mechanistic understanding of the forces impacting the specific CO_2 flux of the SO. Quantifying the different processes influencing the SO's carbon flux is an integral piece in understanding the carbon budget. One critical way to analyze carbon dioxide uptake is by observing phytoplankton blooms.

Phytoplankton blooms are limited by light and nutrients such as iron (Boyd et al., 2000). Notable iron (ref) sources in the Southern Ocean include glacial and iceberg melt (Lannuzel et al., 2016), continental shelf sediment (Gerringa et al., 2012), dust deposition (Weis et al.m 2024), oceanic deposition of atmospheric aerosols (Tang et al. 2021), and bathymetric interactions with the Antarctic Circumpolar Current (Boyd et al., 2010). Being a high-nutrient low chlorophyll zone (HNLC), an area with an abundance of macronutrients but low phytoplankton biomass, phytoplankton blooms rely on a variety of physical processes mentioned prior, and partially on upwelling, another source of nutrients. Upwellings form through high wind events or storms. During a high wind or storm event, enhanced stress on the ocean's surface increases turbulence, resulting in deeper mixing in the ocean's subsurface. The deepening of the mixed-layer depth (MLD) helps replenishing nutrients from the water below. On the contrary, Less stress, or less wind result in shallower MLD.. Nutrients gathered during mixing events are brought to the surface during stratification, light availability increases, and surface temperatures become warmer, creating a favorable environment for phytoplankton to bloom. Observing storm-induced phytoplankton blooms is important when considering the Southern Ocean's carbon flux. Some of this carbon dioxide is exported to the deep ocean via fecal pellets, dead cells, or aggregates, which play a crucial role when quantifying the Southern Ocean's total carbon flux (Iversen, 2023). Storm-induced phytoplankton blooms occur rapidly in the open ocean, which makes them harder to observe.

The vast SO is known for its stormy conditions, limiting ship-based and satellite observations. Biogeochemical (BGC) Argo floats are autonomous floats that measure physical and biogeochemical properties in the ocean. The BGC Argo array provides a way to obtain critical subsurface observations. BGC Argo floats are autonomous floats that provide subsurface physical and biogeochemical observations where other types of observations are restricted. These floats are equipped with sensors to measure temperature, salinity, pH, dissolved oxygen (DO), nitrate (NO_3), downwelling irradiance,

chlorophyll-a (CHLA) fluorescence, and optical particle backscatter (b_{bp}). By utilizing these sensors, we are able to gain a better understanding of the biogeochemical processes occurring in the oceans sub-surface. For example, the NO_3 sensor allows us to view the upwelling of nutrients, and sensors such as CHLA, dissolved oxygen, pH, and b_{bp} allow us to analyze phytoplankton blooms.

In this case study, we analyze changes in the MLD depth in relation to a high wind event. We do this by first searching for a high wind or storm event around a high-frequency (daily profiling) biogeochemical (BGC) Argo float deployed within the Southern Ocean. These floats, deployed by the Southern Ocean Carbon and Climate Observations and Modeling (SOCCOM) and Global Ocean Biogeochemistry Array (GO-BGC) projects, as well as the University of Washington and MBARI, provide us with a gateway to examine phytoplankton blooms in the open ocean.

2 MATERIALS AND METHODS

2.1 BGC-ARGO FLOATS

Data was used from a snapshot from April 26, 2023 provided by Dr.Carranza. The snapshot consists of 34570 profiles across 382 floats from March 2012 to April 2023. Floats in this snapshot were deployed as part of the Southern Ocean Carbon and Climate Observations and Modeling (SOCCOM) project. Only data with ODV QC flag of 0, good data, was used for this study. Floats deployed by the SOCCOM project follow the general profiling routine of drifting for 10 days at 1000m depth prior to descending to their profiling depth. They then ascend to the surface where they transmit data to satellites, and continue the 10 day cycle. To confirm normal sensor operation, however, a float may switch to a higher profiling frequency, profiling roughly daily. Periods of this high-frequency profiling are helpful when analyzing high wind or storm-induced phytoplankton blooms by providing a way to observe rapid changes in sub-surface biogeochemical properties. In order to analyze these events in the SO specifically, we filtered for high frequency profiling floats south of 30°S.

A suite of sensors including temperature, salinity, pH, downwelling irradiance, CHLA fluorescence, b_{bp}, (DO), and NO_3 is equipped on each float. For our analysis, we utilized the CHLA fluorescence, b_{bp}, DO, pH, and temperature sensors. We are able to estimate

PCO_2 from measured pH values, and POC from the measured b_{bp} values (Argo, 2024). We smoothed b_{bp} data by using a 5 point moving median to reduce overestimation of backscatter values caused by white caps and bubbles (Stramski et al., 2004). Unfortunately, the NO_3 sensor on our chosen float malfunctioned, resulting in poor quality and missing data, and was not included in this study.

We calculated the euphotic zone depth by using CHLA with depth data (Morel and Maritorena 2001). Anomalies were calculated by subtracting the measured value from the measured values from the profile before the high frequency profiling period. All measured variables were interpolated every 5m depth from the surface to 100m depth.

We chose one float, WMO 5904693, to use for this study. The chosen float profiled from May 20, 2016 to February 21, 2020, with a trajectory between 56.6380°S, 183.3920°E and 43.3350°S, 250.1210°E. The float switched to high frequency profiling between February 8, 2019 and February 23, 2019, traveling between 53.0780°S, 212.7650°E and 50.9250°S, 214.3370°E.

2.1 STORM TRACKS

Storm tracks from TempestExtremes ERA5 were downloaded, consisting of storm data from January 2016 to December 2020. TempestExtremes uses minimum sea level pressure to track storms (Ullrich and Zarzycki, 2017). We filtered for storms within a 5° latitude and longitude radius of the floats location during its high frequency profiling period, as extratropical cyclones (ETC) in the SO can reach up to 1000km in diameter (Lodise et al., 2022). We then analyzed the timing of the storm's passage in correlation to the change in the measured float variables. After this analysis, we singled out one storm that potentially affected the float. This storm occurred between February 5, 2019 and February 8, 2019, between 63°S, 195.25°E and 55°S, 268.75°E. This storm lies on the poleward side of the float.

2.3 WIND SPEED

We used Cross-Calibrated Multi-Platform (CCMP) Version 2.0 to get collocated wind speed with the floats location. CCMP 2.0 uses winds from Remote Sensing Systems

(Mears et al., 2019). We averaged daily wind speeds for each day during , and +/- 10 days before/after the float's high frequency period. Wind speeds of greater than 10m/s with a persistence of 3 days corresponds to synoptic-scale ETCs that are strong enough to induce ocean mixing. Thus, we defined wind speeds ≥10m/s for at least 3 days as a storm event (Carranza et al., 2024). The main purpose for using these wind speeds is to verify storm events impacting the float, or to verify a high wind event.

3 RESULTS AND DISCUSSION

We located one float (WMO: 5904693) that potentially was influenced by a storm. This float is located in the open ocean southwest of New Zealand. The storm of interest began at 53°S, 195.25°E on February 5, 2019, and moved southwest until February 8, 2019, located at 62.25°S, 268.75°E (Figure 1). Meanwhile, the float hung around 53-50°S, 214-213°E. It is important to note that the median storm size in the southern hemisphere has a radius of 5° latitude and longitude (Lodise et al., 2022); this impact radius is shown in the shaded gray circles around the minimum sea level pressure point.

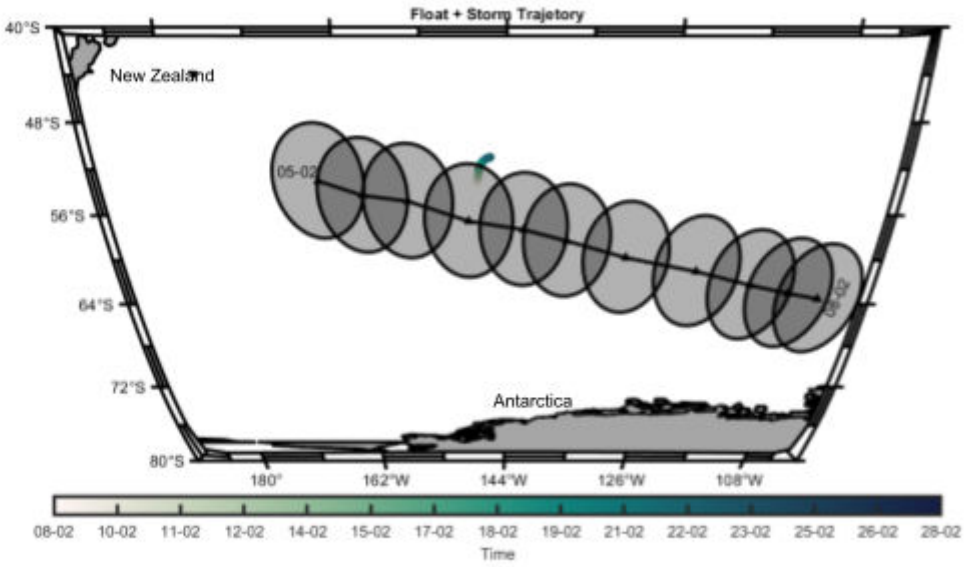

Figure 1: Map of float and storm location. Float location is indicated by the colored markers, storm location is indicated by the black line. The average radius of a storm in the Southern Ocean is outlined in the gray circles around storm location points.

We are unable to assume that the float was directly impacted by the storm shown due to temporal gaps in the storm's passing and the observed phytoplankton bloom. Nevertheless, we still have a high wind event occurring at the float. Below, Figure 2 shows the collocated wind speed for the floats' location. The red line denotes the 10m/s threshold for storm events classified by wind. We found that wind speeds are above the storm threshold for the majority of the high-frequency profiling period. February 19-20, however, marks a time where the winds dramatically decreased in speed, reaching 2m/s.

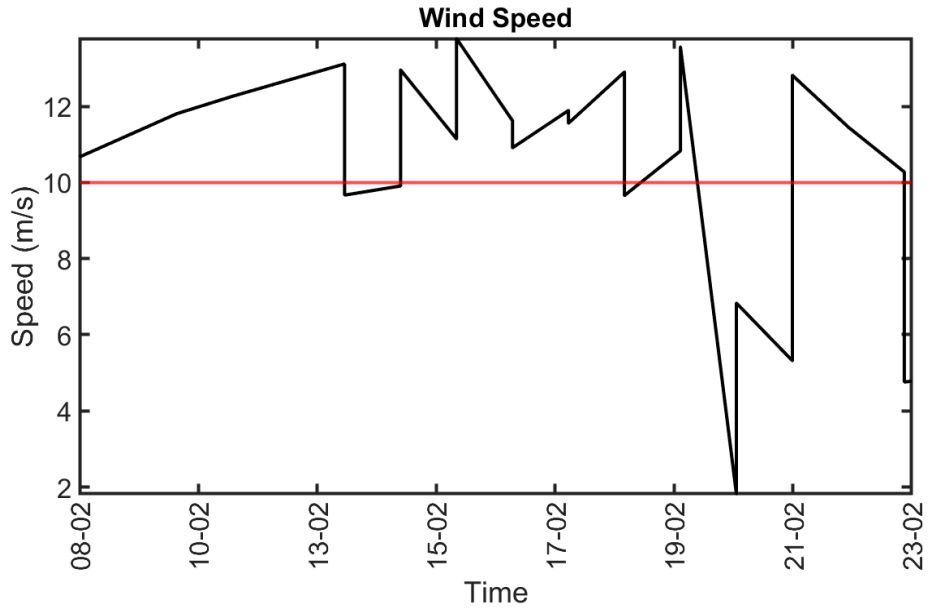

Figure 2: Collocated wind speeds (m/s) with float location during the high frequency profiling period. The common storm threshold of 10m/s is represented by the solid red line.

Since wind speeds were above the storm threshold, we consider this a high wind event. Events such as these have strong ETC force winds that are strong enough to induce vertical ocean mixing. The first indication of an incoming phytoplankton bloom is characterized by a deepening of the MLD with cooling surface temperatures, then subsequent shoaling of the MLD with increasing surface temperatures. Physical changes such as these usually coincide with stronger wind speeds followed by slower wind speeds, a pattern we observe in Figure 2. We notice the signature MLD movement and temperature changes as follows.

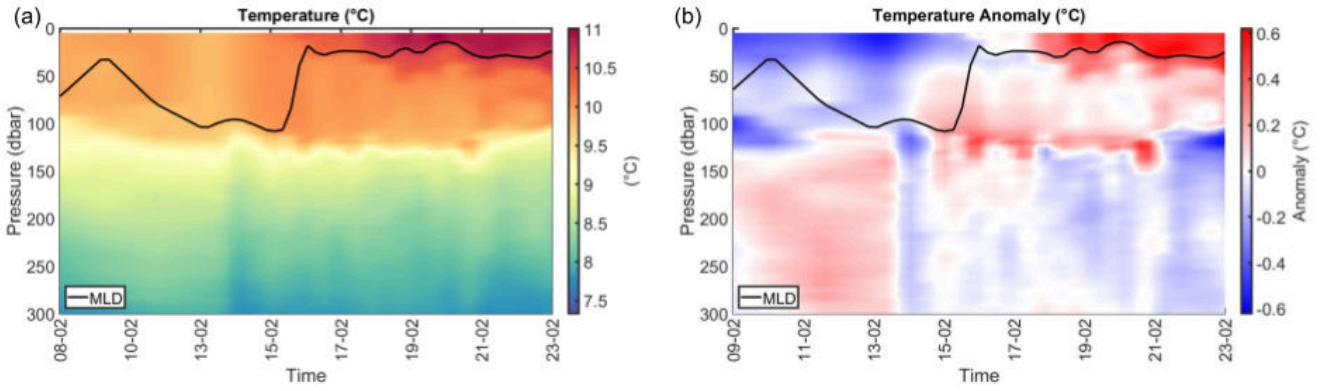

Figure 3: (a)Temperature (°C) profile during the high frequency profiling period. (b) Temperature anomaly (°C) during the high frequency profiling period. The MLD (m) is represented by the black line.

As seen above, the MLD deepens, and remains deep from February 9-14, and then begins the shoaling process February 15th and spends the rest of the high frequency profiling period stabilizing, and reaches its shallowest point on February 19th. Both the temperature plot and temperature anomaly plot (Figure 3) indicate an increase in temperature after the shoaling of the MLD relative to before this profiling period.

We also look into biological variables: CHLA and POC. Below are figures showing the section plots for CHLA and POC (Figure 5) for the high-frequency profiling period. We observe a noticeable increase in CHLA beginning February 19, which lines up with the wind speeds earlier shown. The largest increase in POC lags a little behind the deeper CHLA increase, as POC accumulation relies on phytoplankton growth and formation of aggregates.

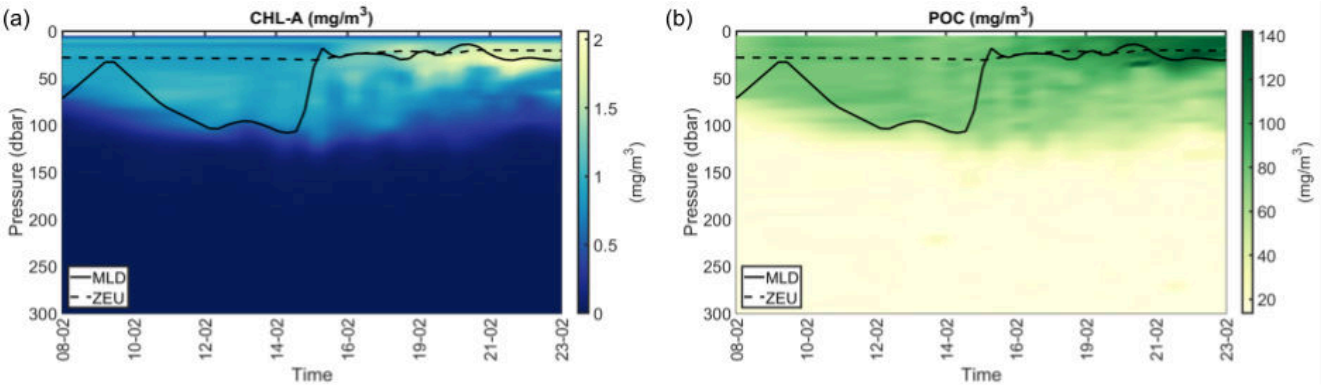

Figure 5: (a) CHLA (mg/m^3) values during the high frequency profiling period. (b) POC (mg/m^3) during the high frequency profiling period. The MLD (m) is represented by the solid black line, and the Z_{eu} (m) is represented by the dashed black line.

In these, and the following, plots, we plotted the Z_{eu}, which is the upper layer of the ocean that receives enough light to support photosynthesis (Soppa et al. 2013). We plot this to verify that the increase in CHLA and POC are due to biological activity, and to differentiate between biological activity and physical processes. The Z_{eu} remains shallow around 25m depth during the bloom, verifying the suggestion of a phytoplankton bloom.

We plotted the CHLA and POC anomalies, shown in Figure 6, to see the difference in these values compared to the values measured in the profile before the high frequency profiling period. We see the strongest positive anomaly beginning on February 19 for both of these variables. This indicates that there was a significant increase in biomass.

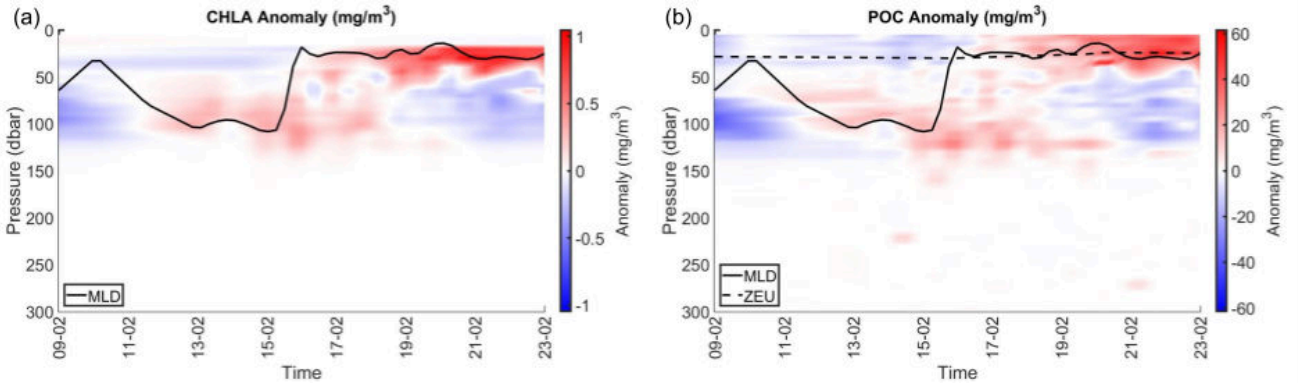

Figure 6: (a) CHLA anomaly (mg/m^3) during the high frequency profiling period. (b) POC anomaly (mg/m^3) during the high frequency profiling period. The MLD (m) is represented by the solid black line, and the Z_{eu} (m) is represented by the dashed black line.

There is a positive DO anomaly, and a negative pCO_2 (Figure 7) anomaly also beginning on February 19. This indicates that there is increased CO_2 uptake and concurrent O_2 release, reflecting enhanced photosynthetic activity. We also observe these features between February 14-20 beginning at 100m depth. We suggest that this is due to detrainment, the process of water, and its properties, being released from the MLD into surrounding water due to it being below the Z_{eu}.

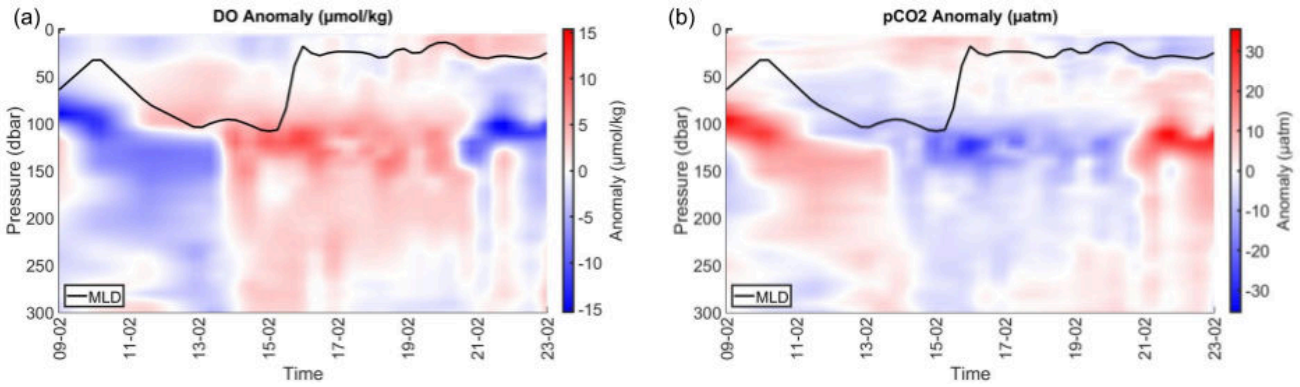

Figure 7: (a) DO anomaly (mg/m^3) for the high frequency profiling period. (b) PCO_2 anomaly (µatm) for the high frequency profiling period. MLD (m) is represented by the solid black line, and the Z_{eu} (m) is represented by the dashed black line.

4 CONCLUSIONS & RECOMMENDATIONS

In this study, we analyzed a high-wind induced phytoplankton bloom through a high frequency BGC Argo float. We noted one potential storm event, but suggest the temporal gap between the storms passing and observed phytoplankton bloom is too great to have significant correlation. However, we do see ETC strength winds at the floats location that we suggest triggered the sub-surface mixing. This study supports the idea that ETC strength winds induce a phytoplankton bloom in the SO due to the MLD movement associated with vertical ocean mixing. We see MLD deepening with storm strength winds, followed by weaker winds and MLD shoaling, which brings nutrients up closer to the surface. This is demonstrated through the different section plots with higher CHLA, POC, and DO, and lower PCO_2 anomalies shortly following the MLD shoaling. This study highlights the critical role of high frequency profiling BGC Argo floats in examining the SO's carbon flux. Only one analyzable event was pinpointed by this study, but other approaches should be taken to reveal and analyze more events.

ACKNOWLEDGEMENTS

I would like to thank my amazing mentors, Guillaume Liniger and Magdalena Carranza, for guiding me through this summer and always helping and supporting me. A huge thank you to George Matsumoto, Megan Bassett, and Jessica Chapman for coordinating

the Internship program, and the fellow interns who all made this summer such a wonderful experience. The MBARI Summer Internship Program is generously supported through a gift from the Dean and Helen Witter Family Fund and the Rentschler Family Fund in memory of former MBARI board member Frank Roberts (1920-2019) and by the David and Lucile Packard Foundation. Additional funding is provided by the Maxwell/Hanrahan Foundation.

References:

Argo. 2025. Argo float data and metadata from Global Data Assembly Centre (Argo GDAC). https://doi.org/10.17882/42182

Boyd PW et al. 2000. A mesoscale phytoplankton bloom in the polar Southern Ocean stimulated by iron fertilization. Nature. 407(6805):695–702. https://doi.org/10.1038/35037500

Carranza MM et al. 2024. Extratropical storms induce carbon outgassing over the Southern Ocean. npj Clim Atmos Sci. 7(1):1–16. https://doi.org/10.1038/s41612-024-00657-7

Gerringa LJA et al. 2012. Iron from melting glaciers fuels the phytoplankton blooms in Amundsen Sea (Southern Ocean): Iron biogeochemistry. Deep Sea Research Part II: Topical Studies in Oceanography. 71–76:16–31. https://doi.org/10.1016/j.dsr2.2012.03.007

Gruber N, Landschützer P, Lovenduski NS. 2019. The Variable Southern Ocean Carbon Sink. Annu Rev Mar Sci. 11(1):159–186. https://doi.org/10.1146/annurev-marine-121916-063407

Iversen MH. 2023. Carbon Export in the Ocean: A Biologist's Perspective. Annu Rev Mar Sci. 15(1):357–381. https://doi.org/10.1146/annurev-marine-032122-035153

Lannuzel D et al. 2016. Iron in sea ice: Review and new insights Deming JW, Miller LA, editors. Elementa: Science of the Anthropocene. 4:000130. https://doi.org/10.12952/journal.elementa.000130

Large WG, Patton EG, Sullivan PP. 2021. The Diurnal Cycle of Entrainment and Detrainment in LES of the Southern Ocean Driven by Observed Surface Fluxes and

Waves. Journal of Physical Oceanography. 51(10):3253–3278. https://doi.org/10.1175/JPO-D-20-0308.1

Lodise J et al. 2022. Global Climatology of Extratropical Cyclones From a New Tracking Approach and Associated Wave Heights From Satellite Radar Altimeter. JGR Oceans. 127(11):e2022JC018925. https://doi.org/10.1029/2022JC018925

Mears CA et al. 2019. A Near‐Real‐Time Version of the Cross‐Calibrated Multiplatform (CCMP) Ocean Surface Wind Velocity Data Set. JGR Oceans. 124(10):6997–7010. https://doi.org/10.1029/2019JC015367

Morel A, Maritorena S. 2001. Bio‐optical properties of oceanic waters: A reappraisal. J Geophys Res. 106(C4):7163–7180. https://doi.org/10.1029/2000JC000319

Sokolov S, Rintoul SR. 2007. On the relationship between fronts of the Antarctic Circumpolar Current and surface chlorophyll concentrations in the Southern Ocean. J Geophys Res. 112(C7):2006JC004072. https://doi.org/10.1029/2006JC004072

Soppa MA, Dinter T, Taylor BB, Bracher A. 2013. Satellite derived euphotic depth in the Southern Ocean: Implications for primary production modelling. Remote Sensing of Environment. 137:198–211. https://doi.org/10.1016/j.rse.2013.06.017

Stramski D, Boss E, Bogucki D, Voss KJ. 2004. The role of seawater constituents in light backscattering in the ocean. Progress in Oceanography. 61(1):27–56. https://doi.org/10.1016/j.pocean.2004.07.001

Ullrich PA, Zarzycki CM. 2017. TempestExtremes: a framework for scale-insensitive pointwise feature tracking on unstructured grids. Geosci Model Dev. 10(3):1069–1090. https://doi.org/10.5194/gmd-10-1069-2017

Weis J et al. 2024. One-third of Southern Ocean productivity is supported by dust deposition. Nature. 629(8012):603–608. https://doi.org/10.1038/s41586-024-07366-4